https://doi.org/10.5194/egusphere-2022-972
Preprint. Discussion started: 1 November 2022

A study of optical scattering modelling for mixed phase Polar Stratospheric Clouds

Francesco Cairo[1], Terry Deshler[2], Luca Di Liberto[1], Andrea Scoccione[3], and Marcel Snels[1]

[1]Istituto di Scienze dell'Atmosfera e del Clima, Consiglio Nazionale delle Ricerche, Rome, Italy
[2]Department of Atmospheric Science, University of Wyoming, Laramie,Wyoming, USA
[3]Centro Operativo per la Meteorologia, Aeronautica Militare, Pomezia, Italy

Correspondence: Francesco Cairo (f.cairo@isac.cnr.it)

Abstract. Scattering codes are used to study the optical properties of Polar Stratospheric Clouds (PSC). Backscattering and extinction can be computed with available scattering codes once the particle size distribution (PSD) is known and a suitable refractive index is assumed. However, PSCs often appear as external mixtures of Supercooled Ternary Solution (STS) droplets, solid Nitric Acid Trihydrate (NAT) and possibly ice particles, making questionable the assumption of a single refractive index and a single morphology to model the scattarers. Here we consider a set of fifteen coincident measurements of PSC above McMurdo Station, Antarctica, by ground-based lidar and balloon-borne Optical Particle Counters (OPC), and in situ observations taken by a laser backscattersonde and an OPC during four balloon stratospheric flights from Kiruna, Sweden. This unique dataset of microphysical and optical observations allows to test the performances of optical scattering models when both spherical and aspherical scatterers of different composition and, possibly, shapes are present.

Here we consider particles as STS if their radius is below a certain threshold value R_{th} and NAT or possibly ice if above it. The refractive indices are assumed known from the literature. Mie scattering is used for the STS, assumed spherical, while scattering from NAT particles, considered as spheroids of different Aspect Ratio (AR), is treated with T-Matrix results where applicable, and of geometric-optics-integral-equation approach where the particle size parameter is too large to allow for a convergence of the T matrix method. The parameters R_{th} and AR of our model are chosen to provide the best match with the observed optical backscattering and depolarization. The comparison of the calculations with the measures is satisfactory for the backscattering but not so for the depolarization, and possible causes are discussed. The results of this work help to understand the limits of the application of these scattering theories in modeling the optical response of particles of different composition and morphology.

1 Introduction

Polar Stratospheric Clouds (PSC) appear in the polar stratosphere during winters due to the very low temperatures and the dynamic isolation of air within the polar stratospheric vortex. They have raised much attention due to the twofold role played in polar stratospheric ozone depletion: providing surfaces for the heterogeneous reactions that lead to the reactivation of chlorine and decreasing the concentration of HNO_3 in the gaseous phase thus altering the balance of the chlorine activation/deactivation cycles (Solomon, 1988). A comprehensive review of studies and knowledge acquired can be found in Tritscher et al. (2021).

https://doi.org/10.5194/egusphere-2022-972
Preprint. Discussion started: 1 November 2022

PSCs can either be formed of liquid droplets composed of supercooled ternary solutions (STS) of sulfuric acid, nitric acid and water, or solid nitric acid trihydrates (NAT), the thermodynamically stable form of HNO_3 and H_2O in the polar stratosphere, or possibly - when temperature is low enough - ice. Initially PSCs were classified as three types based on lidar measurements of the intensity of the backscattered light and the amount of depolarization of the returned signals (Browell et al., 1990). With the accumulation of observations, it has been realized that it is not common to observe a PSC of a well defined type (Pitts et al., 2018b). More often PSCs appear as external mixtures of liquid STS droplets, NAT, and/or ice, depending on the thermal history that led to their formation. For example, it is believed that the nucleation of NAT could start in droplets of a pre-existing population of STS, but not all liquid droplets may convert into solid NATs, allowing the coexistence of particles of different composition and phases and thus of intermediate optical characteristics (Peter and Grooß, 2012).

The existence of multi-phase PSC with particles of different shapes and composition, henceforth with different particle refractive indices, makes the modeling of the scattering characteristics of the cloud problematic. While Mie scattering theory has been used to analyse PSCs consisting of spherical particles (Toon et al., 2000), detailed analysis of observations of different classes of PSCs (Deshler et al., 2000) may be questionable because they may consist of non spherical solid particles with sizes comparable to the wavelength of the laser, and hence the results may be hampered by biases due to the unverified assumption of spherical scatteres. Because of this, some studies have chosen to limit themselves to liquid clouds only (Jumelet et al., 2008), or to make an effort and use theoretical modelling of light scattering for aspherical scatterers in the analysis. A viable solutions which is not so demanding in terms of computational effort is the use of T-Matrix theory (see Liu and Mishchenko (2001), and references within). T-Matrix method is an exact technique for the computation of nonspherical scattering based on a direct solution of Maxwell's equations assuming homogeneous, rotationally symmetric non spherical particles or clusters of spheres (Mishchenko et al., 1996), and T-Matrix codes are orders of magnitude faster than other approaches used in particle light scattering, like the Discrete Dipole Approximation (Singham and Salzman, 1986) and the Finite Difference Time Domain (Yang and Liou, 1996a) techniques. The T-Matrix approach to compare microphysical and optical observations has been used in a number of cases (Voigt et al., 2003; Scarchilli et al., 2005), under the assumption of particles as prolate or oblate spheroids. However even this approach could be controversial given that, just as solid particles cannot be modeled as spheres, for similar reasons it is debatable that they can be modeled as spheroids, and biases can arise under that assumption as well. For instance, Reichardt et al. (2002) showed how under the hypothesis of spheroidal particle shapes, surface area density and volume density of leewave PSCs are systematically smaller by, respectively, 10–30% and 5–25% than the values found for mixtures of droplets, asymmetric polyhedra, and hexagons. Furthermore, there is no clear indication on what kind of aspect ratio can be univocally assumed for the spheroidal case (Reichardt et al., 2004; Engel et al., 2013; Woiwode et al., 2016). Finally, T-Matrix codes suffer from convergence problems beyond a few dozen size parameters, especially for extreme aspect ratios.(Mishchenko and Travis, 1998)

Given that there is still no completely satisfactory solution to tackle scattering from solid PSC particles due to the ambiguities that still persist about their shape, the use of Mie theory continues to be attractive and is used widely despite the unverified hypothesis of spherical diffusers. The speed of computation it offers is advantageous when used for statistical or climatological studies (Pitts et al., 2009, 2013), or when optical properties less dependent on the assumption of sphericity have to be calculated,

https://doi.org/10.5194/egusphere-2022-972
Preprint. Discussion started: 1 November 2022

as is in the case of extinction (David et al., 2012; Daerden et al., 2007). In PSC studies, Mie theory was also sometimes used to simulate aspheric particulate backscattering, employing corrections that take into account its reduction due to the asphericity of the scatterers (Snels et al., 2021; Cairo et al., 2022). However, the Mie theory cannot produce depolarized backscattering and attempts with simple empirical models to use it to mimic depolarization from aspherical particles does a very poor job in reproducing the measured depolarization (Cairo et al., 2022).

The aim of our study is to employ concomitant microphysical and optical measurements of PSCs when both liquid and solid particles are present and compare these with optical scattering computations done with codes capable of reproducing depolarization in backscattering. This allows us to verify the capacities and limits of these codes, tested on a relevant data set which provides both microphysical and optical measurements of mixed-phase particulate distributions. The methodology illustrated is not restricted to the study of mixed phase PSCs, but can find applications in all those cases in which the aerosol appears as an external mixture of solid and liquid particles, distinguishable on the basis of their different typical sizes.

2 Data and Methods

2.1 Dataset

We have analysed fifteen measurements of PSC optical parameters observed by a groundbased lidar, coincident with microphysical observations acquired by a balloon-borne Optical Particle Counter (OPC). These observations were taken above McMurdo Station, Antarctica, between 1994 and 1999 (Snels et al., 2021). In addition we analysed four in situ balloonborne observations carried out by a laser backscattersonde and an OPC during 4 stratospheric balloon flights from Kiruna, Sweden, between 2000 and 2002 (Weisser et al., 2006). The Antarctic lidar and balloonborne OPC dataset has been extensively discussed in Snels et al. (2021) where it has been used to provide empirical relations linking particle Surface Area and Volume densities with the backscatter coefficients. The main characteristics of the instrumentation will be here only briefly recalled.

The lidar observations have been provided by a system detecting 532 nm backscattered light with parallel and perpendicular polarization with respect to the linear polarization of the emitting laser (Di Donfrancesco et al., 2000), thus allowing the measurement of Backscatter Ratio BR, Volume Depolarization δ and Aerosol Depolarization δ_A from 10 to 23 km. These optical parameters follows the usual definitions (Cairo et al., 1999); in the following the subscripts mol and A denote respectively the molecular and particle contribution to the optical coefficients, and $cross$ and par denote the perpendicular and parallel polarization of the Backscatter Coefficient β (Collis and Russell, 1976).

$$BR = \frac{\beta_A^{cross} + \beta_{mol}^{cross} + \beta_A^{par} + \beta_{mol}^{par}}{\beta_{mol}^{cross} + \beta_{mol}^{par}} \tag{1}$$

$$\delta = \frac{\beta_{mol}^{cross} + \beta_A^{cross}}{\beta_{mol}^{par} + \beta_A^{par}} \tag{2}$$

$$\delta_A = \frac{\beta_A^{cross}}{\beta_A^{par}} \tag{3}$$

$$\tag{4}$$

https://doi.org/10.5194/egusphere-2022-972
Preprint. Discussion started: 1 November 2022

An alternative definition of Total Volume Depolarization δ_T and Total Aerosol Depolarization δ_{TA} will also be used in the following and is here introduced as:

$$\delta_T = \frac{\beta_A^{cross} + \beta_{mol}^{cross}}{\beta_A^{cross} + \beta_{mol}^{cross} + \beta_A^{par} + \beta_{mol}^{par}} \tag{5}$$

$$\delta_{TA} = \frac{\beta_A^{cross}}{\beta_A^{par} + \beta_A^{cross}} \tag{6}$$

$$\tag{7}$$

being:

$$\delta_T = \frac{\delta}{\delta + 1} \tag{8}$$

The formulas for switching from one to the other can be found in Cairo et al. (1999).

The BR is retrieved using the Klett algorithm where the attenuation correction follows Gobbi (1995). The δ is calibrated with the method described in Snels et al. (2009). Uncertainties in BR are estimated to be 5% while uncertainty in δ_A is about 10-15% (Adriani et al., 2004). Typical measurements are 30–60 min integration over the signal, and the vertical resolution is 75 m in 1994 and 1995 and 225 m in the other years. The OPC, which makes 10 second measurements, corresponding to roughly 50 meter vertical resolution, has been averaged to 250 meter bins. For comparison with the lidar the OPC has been interpolated onto the vertical grid of the lidar.

The OPC is described in Hofmann and Deshler (1991) and Deshler et al. (2003a). A throughful revision of its dataset is presented in Deshler et al. (2019). The instrument uses white light to measure scattering at 40° in the forward direction from particles passing through a dark field microscope. Mie theory and a model of the OPC response function are used to determine particle size throughout the range from 0.19 to 10.0 μm radius. The OPC provides time series of size resolved particle concentration histograms at 8 to 12 size bins, depending on the instrument used. A measurement of total concentration of particles is simultaneously determined by a CN counter close to the OPC, which grows all particles larger than 0.01 μm to an optically detectable size and counts them (Campbell and Deshler, 2014). Particle size histograms are fitted to unimodal or bimodal lognormal size distributions, which are the representation of size distribution used in this work.

A series of balloon launches were carried out from Kiruna, Sweden in the early 2000s. The payload included, among other instruments and in addition to the OPC and the CN, a backscattersonde capable of measuring in situ backscattering and depolarization at 532 nm with 10 seconds time resolution. Details of such instrument are presented in Adriani et al. (1999) and Buontempo et al. (2009). Here we use data from four flights that took place on 19 January 2000 (Voigt et al., 2003), 9 December 2001 (Deshler et al., 2003b), 4 and 6 December 2002 (Larsen et al., 2004; Weisser et al., 2006). As these balloon flights were not simple ascents like the antarctic ones, but were commanded to perform altitude changes, by deflating the balloon or releasing ballast, to maximize the transit time in the detected PSCs, the backscattersonde data have been interpolated to the OPC 250 m average of the data, corrisponding to a time grid spacing of 60 or 75 seconds depending on flight.

In our study each data point includes the values of BR, δ_A and of the PSD defined by the three or six parameters of a mono or bimodal lognormal distributions. Altitude, pressure and temperature are also present as ancillary data. We identify a data

https://doi.org/10.5194/egusphere-2022-972
Preprint. Discussion started: 1 November 2022

point as a PSC observation when the BR is greater than 1.2 and the temperature at the observation is below 200 K. Moreover, to select the presence of mixed phase clouds, we require that β_A^{cross} is greater than 5 $10^{-6} km^{-1} sr^{-1}$. Under these condition, a total of 141 data point from the Antarctic and 332 data point from the Arctic flights have been selected for the study.

2.2 Optical model

While the nucleation of NAT and ice is a threshold process, STS particles can grow upon cooling from the the ubiquitous liquid Stratospheric Sulphate Aerosol (SSA), by continuously taking up nitric acid and water from the gas phase. They form droplets with volumes varying with temperatures but nevertheless with larger number density and smaller particle dimensions than NAT. Conversely, NAT particles are expected to be of smaller number density, but with dimension that can easily grow larger than the average STS particle radius of a few tenths of μm (Carslaw et al., 1997; Grooß et al., 2014) due to the smaller saturation vapour pressure of the nitric acid with respect to them. Deshler et al. (2003b) provide direct observations of this separation between STS and NAT. All the more reason, due to the larger availability of water vapor, ice particles can grow even larger, often with linear dimensions exceeding 4–5 μm (Tritscher et al., 2019).

In our study we make use of the fact that in a mixed phase PSC the large particles are likely NAT or ice, solid particles which depolarize the backscatter light, while the small ones are liquid STS, that is spherical, and do not depolarize the backscattering. Figure 1 shows our dataset mapped in terms of the BR - as 1-1/BR for the sake of plot readability - and δ_A and colour coded with respect to the fraction of particles larger than 1 μm in radius, with respect to the total number of particles. As can be seen, it is a general feature that for each BR value, higher depolarization values are associated with higher fractions of large particles. Noteworthy, at high BR, high fractions of large particles are associated with depolarizations which, albeit high, are smaller than those observed at medium-low BR. In fact those depolarizations at medium-low BR are associated with lower ratios of big to small particles. In other words, although at medium-low BR the large particles are proportionally less numerous than at high BR, the depolarization in the former case is higher. It has also to be noted in the plot that, in the high BR range at 1-1/BR=0.8, there are a few cases where high depolarization is associated with a low fracton of large particles. In these cases, although the relative abundance of large particles was low, the particles were unusually large, exceeding few μm. These very large particles, although in small concentrations, are causing the high depolarization observed. The temperature in these few cases was however high enough to exclude them as ice particles.

We plan to consider particles as STS when their radius is below a threshold value R_{th} and NAT above it. We use values of 1.44, and 1.48 for the refractive index of, respectively, STS, and NAT. These values are compatible with the large PSC data set produced by the CALIPSO observations (Hoyle et al., 2013; Pitts et al., 2018a) and fall within the estimates presented for STS and NAT (Adriani et al., 1995; Deshler et al., 2000; Scarchilli et al., 2005). For completeness, ice particles are considered when radii are larger than 4 μm and temperatures fall below 185 K. This happens only in 10% of the total dataset. In those few cases a value of 1.31 is used (Kokhanovsky, 2004).

For each data point, we split the PSD into two branches, namely $PSD_{STS} = PSD(r < R_{th})$ and $PSD_{asph} = PSD(r > R_{th})$. As stated, the presence of ice particles is taken into consideration by inspecting the temperature T observed at the measurement, so if $T > T_{ICE}$ we pose $PSD_{NAT} = PSD_{asph}(r > R_{th})$, while if $T < T_{ICE}$ we limit the presence of NAT

https://doi.org/10.5194/egusphere-2022-972
Preprint. Discussion started: 1 November 2022

particles at radii smaller than 4μm, i.e. $PSD_{NAT} = PSD_{asph}(R_{th} < r < 4\mu\text{m})$ and consider as ice the particles with bigger radii, $PSD_{ICE} = PSD_{asph}(r > 4\mu\text{m})$.

The backscattering coefficients and depolarization ratio for the STS, NAT and ice particles are separately computed. For STS we have used a Mie code (Bohren and Huffman, 2008), available from the NASA's OceanColor Web site. For NAT and ice we have used the GRASP (Generalized Retrieval of Aerosol and Surface Properties) Spheroid Package. GRASP is the first unified algorithm developed for characterizing atmospheric properties gathered from a variety of remote sensing observations (Dubovik et al., 2014), whose software packages are available on the Web. The Spheroid Package allows fast, fairly accurate, and flexible modelling of single scattering properties by randomly oriented spheroids with different size and shape. It includes a software and kernels data base. The details of the scientific concept are described in the paper by Dubovik et al. (2006). The kernel look-up tables include results of calculations using T-Matrix code where convergence was acquired, and when convergence was not achieved, the geometric-optics-integral-equation approach (Yang and Liou, 1996b, 2006) was used, that is expected to provide accurate optical characteristics for spheroids with size parameter larger than 30 – 40. The two methods have been shown to produce comparable results over the size range in which both are applicable (Dubovik et al., 2006). Thus, the software and kernels data base provide the kernel matrices for randomly oriented spheroids with Aspect Ratios (AR) from ~ 0.3 (flattened spheroids) to ~ 3.0 (elongated spheroids) and covering the size parameter range from ~ 0.012 to ~ 625 (when a wavelenght of 0.44 is used) for a wide range of particle refractive index.

The total particle backscattering from the particles of the PSD can thus be parametrized with R_{th} and AR and written as:

$$\beta_A = \beta_A(R_{th}; AR) = \beta_{STS}(R_{th}) + \beta_{NAT}(R_{th}; AR) + \beta_{ICE}(R_{th}; AR) \tag{9}$$

Here we have used for the sake of simplicity the same AR for NAT and ice. Even if this hypothesis were not fully verified, this should not impact severely our study, as only 10% of our observations have temperatures below 185 K, and no definite ice observations could be clearly discerned in our database. Now, the particle depolarization δ_A can be parametrized in terms of AR and R_{th} as well and be written as a weighted average of the contributions from the different classes of particles:

$$\delta_A = \delta_A(R_{th}; AR) = \frac{\beta_{NAT}(R_{th}; AR) \cdot \delta_{A,NAT}(R_{th}; AR) + \beta_{ICE}(R_{th}; AR) \cdot \delta_{A,ICE}(R_{th}; AR)}{\beta_A(R_{th}; AR)} \tag{10}$$

It is useful here to recap how scattering from aspheric particles changes, compared to Mie theory, when T-Matrix is used. Obviously, Mie theory cannot reproduce the depolarized backscattering typical of aspherical scatterers. According to T-Matrix, the depolarization is negligible for scatterers size parameters lower than unity (given the waveleght used in our study, this corresponds to particle radius approximately below 0.1 μm), it grows up to a maximum that is reached for size parameters of the order of ten (i.e. particle radius around 1 μm) and then decreases towards an asymptotic value for size parameters greater than one hundred (particle radius greater than 10 μm). Both the maximum value and the asymptotic value vary according to the AR considered. In particular, the asymptotic value of the depolarization can assume values from 10% to 40%, and the maximum value from 30% to 80%, the two variabilities are not connected. The dependence of the single particle depolarization on shape and size has been studied extensively by Liu and Mishchenko (2001). It has to be stressed that there is no simple relationship that binds the peak and asymptotic depolarization values to the AR of the particle, although there is a general

https://doi.org/10.5194/egusphere-2022-972
Preprint. Discussion started: 1 November 2022

tendency for small AR values to give large asymptotic depolarization values, and for large AR values to produce medium asymptotic depolarization values. The backscattering itself reproduces the Mie results for size parameters below unity, then is progressively reduced to values that can even be one third of the Mie value when the particle size parameters is above ten, again this reduction depends in no simple way on the value of AR.

2.3 Variability with the threshold radius R_{th} and Aspect Ratio AR

We have computed $\beta_A(R_{th}; AR)$ and $\delta_A(R_{th}; AR)$ for a set of threshold radii R_{th} and Aspect Ratios AR ranging respectively from 0.25 to 2 μm and from 0.3 to 3. To find the values that provide the best match with the measured ones β_A^{meas} and δ_A^{meas}, we have calculated the respective Root Mean Squared Errors (RMSE), as:

$$RMSE_{\beta_A} = \sqrt{\frac{\sum_{i=1}^{n}(\beta_{Ai} - \beta_{Ai}^{meas})^2}{n}} \tag{11}$$

$$RMSE_{\delta_A} = \sqrt{\frac{\sum_{i=1}^{n}(\delta_{Ai} - \delta_{Ai}^{meas})^2}{n}} \tag{12}$$

where the index i runs over our dataset. Covariance has also been computed resulting to be everywhere close to zero, except for R_{th} smaller than 0.5 μm, where it resulted positive for AR between 0.5 and 1.5 (and close to unity for AR=1.25), while it was slightly negative (correlation between -0.3 and 0) for AR smaller than 0.5 and greater than 1.5. Since the range of variability of β_A is two orders of magnitude, to estimate the goodness of the agreement independently of the magnitude of β_A, we have also calculated the Root Mean Squared relative Error (ReRMSE), defined as:

$$ReRMSE_{\beta_A} = \sqrt{\frac{1}{n}\sum_{i=1}^{n}\left(\frac{\beta_{Ai} - \beta_{Ai}^{meas}}{\beta_{Ai}^{meas}}\right)^2} \tag{13}$$

$$ReRMSE_{\delta_A} = \sqrt{\frac{1}{n}\sum_{i=1}^{n}\left(\frac{\delta_{Ai} - \delta_{Ai}^{meas}}{\delta_{Ai}^{meas}}\right)^2} \tag{14}$$

Figures 2 and 3 reports the color coded RMSEs, (upper panel) and ReRMSEs (lower panel), with respect to the threshold radius R_{th} and the Aspect Ratio AR.

3 Results

The plots reported in figure 2 and 3 provide suggestions to select the choice of R_{th} and AR to provide the best match between computations and observations. The comparison between the RMSE and RreRMSE for β_A shows similar features: both plots suggest to avoid AR values between 0.6 and 1.5 when an R_{th} below 1 μm is considered, and show similar minimum differences between model and observations for AR below 0.5 and above 1.5. In this range of variability for AR, the R_{th}s that reach the best agreement between model and observations are between 0.25 and 1 μm. The analysis of the RMSE and ReRMSE for δ_A clearly shows regions where the agreement model-experiment is really poor, namely for AR below 0.75 and above 1.25 when R_{th} is below 0.75 μm. Noteworthy, these regions only partially coincide with those of disagreement for β_A. However, for δ_A

https://doi.org/10.5194/egusphere-2022-972
Preprint. Discussion started: 1 November 2022

in relative terms the agreement is unsatisfactory practically everywhere, the relative error being considerably higher than in the case of the comparison of β_A. Regions in which the agreement seems better are those with R_{th} greater than 0.75 μm and AR values below 0.75 or greater than 1.5.

If we look for a compromise that ensures at the same time a good accord between model and data for both β_A and δ_A, the analysis do suggest to maintain R_{th} between 0.75 and 1.25 μm, and keep the AR above 1.5, or below 0.5. Given those constrains, even if an unambiguous choice is not possible, it seems reasonable to pose R_{th} = 1.0 μm and test the two cases for oblate or prolate spheroids, posing AR = 2 .0 and 0.5 respectively, to test the goodness of the agreement. These values meet what we can also expect from what we know about PSC microphysics (Voigt et al., 2000) and about the comparison between backscattering from spherical and scattering from aspherical vs spherical particles (Mishchenko, 2009). With this choice we can present in figures 4 and 5 the scatterplot β_A and δ_A measured vs computed. The upper panels represent the oblate case, the lower the prolate one.

4 Discussion

Figure 4 reporting the scatterplot of measured vs modelled β_A, colour coded in terms of δ_A, represent the analogue of figure 4 in Snels et al. (2021), where in the present case we have used a larger dataset, including Arctic balloon flights, and used T-Matrix instead of a factor 0.5 reduction, common to all particle sizes, for the Mie backscattering computation. In the present case, both for prolate and oblate spheroids, the model is able to reproduce the observations for β_A. While the agreement between calculations and measurements can be considered just fine for β_A with the exception $\beta < 4 \cdot 10^{-5} km^{-1} sr^{-1}$ where the calculations underestimate the measurements, it is not so for δ_A as can be clearly seen from figure 5 where the points are colour coded in terms of β_A. In that case, although there is some tendency to align the points along the diagonal, the dispersion of the points is very large. We can certainly invoke a noisiness in the data, which is present in the δ_A measurements to a larger extent than in the β_A. Moreover, another critical aspect of this analysis is that aspherical particles passing through the OPC will scatter differently than a sphere of the same size, assumed in the OPC retrieval, and this causes an additional uncertainty on the particle true size. However it is likely that the lack of agreement has more profound reasons and that the assumptions made in the construction of our optical model are not fully reflected by reality. It is possible that spheroids are not able to fully replicate the scattering properties of PSC particles. Um and McFarquhar (2011) used geometric ray-tracing codes on ice particles of linear dimension of few tens of μm and showed that differences in the backward scattering between different shape models (Chebyshev particles, Gaussian random spheres, and droxtals) are higher than 100%. Moreover it is possible that the assumption of the same value for the AR for each particle, irrespective of its composition or size, can not hold; on the contrary is quite possible that particle shape changes with the size due to the differential condensational growth along preferred dimensions. In fact, laboratory studies (Grothe et al., 2006), have showed that synthesized aspherical NAT develops different morphologies depending on the growth conditions. The situation is even more complicated for ice particles, of which the extreme variety of shape is known, even in the case of pristine crystals whose morphology is influenced by the air temperature, atmospheric pressure, ventilation and ice supersaturation (Heymsfield et al., 2017).

https://doi.org/10.5194/egusphere-2022-972
Preprint. Discussion started: 1 November 2022

We have seen that different shapes produce different polarization, according to T-Matrix. This has also been proven experimentally since the early works of Sassen and Hsueh (1998) and Freudenthaler et al. (1996) that showed how the lidar depolarization ratio in persisting contrails ranged from 10% to 70%, depending on the stage of their growth and on temperature.

The oversimplified assumption of a common AR for all solid particles is one probable reason why the optical model behaves so poorly in the simulation of depolarization.

To further investigate the causes of this mismatch we turn to the study of the climatology of PSC observations collected from McMurdo's lidar. The measurement of a PSC composed exclusively of solid particles is a rare and above all uncertain event, as we can never be completely certain of the absence of liquid aerosols. However, Adachi et al. (2001) demonstrated that in a plot showing the Total Volume Depolarization δ_T towards 1-1/BR, the experimental points of solid, liquid or variously mixed PSCs are distributed within a triangle whose vertices are 0, δ_{TA}^{asph} and δ_{mol}. These vertexes represent respectively the value of δ_T in the case of pure liquid clouds and pure solid clouds for $BR = \infty$, when the δ_T coincides with δ_{TA} , and in the case when no particles are present i.e. when δ_T attains its molecular value δ_{mol} (Young, 1980). Hence the extrapolated intercept on the y axis at $BR = \infty$ is precisely δ_{TA}^{asph}. This procedure allows us to estimate this asimptotic value. This requires the assumption that the experimental points that fill the triangle of vertices defined above represent PSC observations in mixed phase in which all solid particles share the same aerosol depolarization. Alternatively, one can interpret differently the presence of the datapoints filling the triangle. These points may as well represent single phase PSC of solid particles but with different shapes, hence producing various and different depolarizations.

Figure 6 reports a 2D-histogram of δ_{TA} towards 1-1/BR from twelwe years of lidar observations from 1990 to 2002 in the antarctic station of McMurdo (Adriani et al., 2004). Despite the dispersion of the experimental points, a value close to 40% for δ_{TA}^{asph} can be tentatively assumed - the corrisponding value for δ_A being 67% according to (6).

If we assume that the failure of our model to reproduce the observed depolarization is due to the incorrect assumption of a common AR for all solid particles, we are led to interpret figure 6 admitting that the experimental points filling the triangle of vertices 0, δ_{TA}^{asph} and δ_{mol} represent both PSC in various degrees of mixed phase, and PSC in purely solid phase but composed of particles of various and unidentical shapes. These various shapes give rise to different δ_{TA}. Thus the found value of δ_{TA}^{asph} at the vertex of the triangle, it must not be considered as the univocal value of the depolarization for a PSC in a totally solid phase, but as the maximum of the possible depolarizations obtainable from solid phase clouds, depending on the many possible shapes that the particulate can assume.

Despite the failure to correctly reproduce the observed depolarization, the simulation of the backscattering gives a good indication on the size transition at which cloud particles may begin to be considered NATs, confirming the common wisdom on the microphysics of mixed NAT/STS clouds.

https://doi.org/10.5194/egusphere-2022-972
Preprint. Discussion started: 1 November 2022

5 Conclusions

We have used an optical model to compute with T-Matrix theory the backscatter and depolarization of mixed phase PSC. The model assumes that: i. PSC particles are solid (NAT or possibly ice) above a threshold radius R_{th}, liquid (STS) below; ii. A single shape is common to all solid partiles irrespective of their size or composition. We have tested the model using a data set of coincident lidar, backscattersonde and OPC measurements from Antarctica and Arctic balloon flights.

The analysis suggested the range of optimal R_{th} and AR parameters that best mach the observations. While the agreement between modeled and measured backscatter is reasonable, it is poor for depolarization. Albeit it cannot be excluded a defective accuracy in depolarization data that prevent to fully demonstrate the validity of our model, the most likely reason is an oversimplification in the hypothesis of a common shape for all the solid particles present in the size distribution. However, the result for the backscatter coefficient simulation allows to constrain the model parameters R_{th} and AR into reasonable ranges and should be regarded as the positive result of the study.

The illustrated method can find application in other cases of externally mixed aerosols with coexistence of different phases, where the phases can be distinguished on the basis of the particle size.

Code and data availability. The Mcmurdo lidar data are available at the NDACC web site
ftp://ftp.cpc.ncep.noaa.gov/ndacc/station/mcmurdo/ames/lidar/.
The OPC data files and size distributions are reported at the web site hosting the Wyoming in situ data
http://www-das.uwyo.edu/∼deshler/Data/Aer_Meas_Wy_read_me.htm
and can be downloaded from
ftp://cat.uwyo.edu/pub/permanent/balloon/Aerosol_InSitu_Meas/Ant_McMur.
The arctic balloonborne backscattersonde data are available from the author upon request.
The software for Mie computation is available at:
https://oceancolor.gsfc.nasa.gov/docs/ocssw/bhmie_8py_source.html
The Spheroid Package of the software GRASP is available at:
https://www.grasp-open.com/products/spheroid-package-release/

Author contributions. FC was responsible for most of the writing, review and editing process, supported by all co-authors. FC and MS share the idea behind the article and the data analysis work. MB helped in software development. TD provided OPC data and PSD analysis. LDL and AS provided for the identification and quality check of the dataset.

Competing interests. No competing interests are present

https://doi.org/10.5194/egusphere-2022-972
Preprint. Discussion started: 1 November 2022

Acknowledgements. The authors acknowledge the financial support by PNRA in the framework of the projects POAS (Particles and Ozone in the Stratosphere of Antarctica) and ACLIM (Antarctic Clouds Investigation by Multi-instrument measurements and modeling). The OPC measurements were supported by awards from the US National Science Foundation (NSF) which include OPP award numbers 9615198, 9980594, and Arctic sciences award 0095158. Terry Deshler and Luca Di Liberto acknowledge a grant from the Short-Time-Mobility program of CNR, respectively in 2016 and 2009. The arctic balloon flights were supported by the Commission of the European Union through the Environment and Climate Program (contract ENV4-CT97-0523) and through the CIPA program (EVK2-CT-2000-00095).

https://doi.org/10.5194/egusphere-2022-972
Preprint. Discussion started: 1 November 2022

References

Adachi, H., Shibata, T., Iwasaka, Y., and Fujiwara, M.: Calibration method for the lidar-observed stratospheric depolarization ratio in the presence of liquid aerosol particles, Appl. Opt., 40, 6587–6595, https://doi.org/10.1364/AO.40.006587, 2001.

Adriani, A., Deshler, T., Donfrancesco, G. D., and Gobbi, G. P.: Polar stratospheric clouds and volcanic aerosol during spring 1992 over McMurdo Station, Antarctica: Lidar and particle counter comparisons, Journal of Geophysical Research: Atmospheres, 100, 25 877–25 897, https://doi.org/https://doi.org/10.1029/95JD02029, 1995.

Adriani, A., Cairo, F., Viterbini, M., Mandolini, S., Pulvirenti, L., and Donfrancesco, G. D.: Multiwavelength Aerosol Scatterometer for Airborne Experiments to Study the Optical Properties of Stratospheric Aerosol, Journal of Atmospheric and Oceanic Technology, 16, 1329 – 1336, https://doi.org/10.1175/1520-0426(1999)016<1329:MASFAE>2.0.CO;2, 1999.

Adriani, A., Massoli, P., Di Donfrancesco, G., Cairo, F., Moriconi, M. L., and Snels, M.: Climatology of polar stratospheric clouds based on lidar observations from 1993 to 2001 over McMurdo Station, Antarctica, Journal of Geophysical Research: Atmospheres, 109, https://doi.org/https://doi.org/10.1029/2004JD004800, 2004.

Bohren, C. F. and Huffman, D. R.: Absorption and scattering of light by small particles, John Wiley & Sons, 2008.

Browell, E., Ismail, S., Carter, A., Higdon, S., Butler, C., Robinette, P., Toon, O., and Schoeberl, M.: Airborne lidar observations in the wintertime Arctic stratosphere - Polar stratospheric clouds, Geophysical Research Letters, 17, https://doi.org/10.1029/GL017i004p00385, 1990.

Buontempo, C., Cairo, F., Donfrancesco, G., Morbidini, R., Viterbini, M., and Adriani, A.: Optical measurements of atmospheric particles from airborne platforms: In situ and remote sensing instruments for balloons and aircrafts, Annals of Geophysics, 49, https://doi.org/10.4401/ag-3149, 2009.

Cairo, F., Donfrancesco, G. D., Adriani, A., Pulvirenti, L., and Fierli, F.: Comparison of various linear depolarization parameters measured by lidar, Appl. Opt., 38, 4425–4432, https://doi.org/10.1364/AO.38.004425, 1999.

Cairo, F., Deshler, T., Di Liberto, L., Scoccione, A., and Snels, M.: A study of Mie scattering modelling for mixed phase Polar Stratospheric Clouds, Atmospheric Measurement Techniques Discussions, 2022, 1–17, https://doi.org/10.5194/amt-2022-28, 2022.

Campbell, P. and Deshler, T.: Condensation nuclei measurements in the midlatitude (1982–2012) and Antarctic (1986–2010) stratosphere between 20 and 35 km, Journal of Geophysical Research: Atmospheres, 119, https://doi.org/10.1002/2013JD019710, 2014.

Carslaw, K. S., Peter, T., and Clegg, S. L.: Modeling the composition of liquid stratospheric aerosols, Reviews of Geophysics, 35, 125–154, https://doi.org/https://doi.org/10.1029/97RG00078, 1997.

Collis, R. and Russell, P.: Lidar measurement of particles and gases by elastic backscattering and differential absorption, in: Laser monitoring of the atmosphere, pp. 71–151, Springer, 1976.

Daerden, F., Larsen, N., Chabrillat, S., Errera, Q., S, B., Fonteyn, D., K, H., and M, F.: A 3D-CTM with detailed online PSC-microphysics: Analysis of the Antarctic winter 2003 by comparison with satellite observations, Atmospheric Chemistry and Physics, 7, https://doi.org/10.5194/acpd-6-8511-2006, 2007.

David, C., Haefele, A., Keckhut, P., Marchand, M., Jumelet, J., Leblanc, T., Cenac, C., Laqui, C., Porteneuve, J., Haeffelin, M., Courcoux, Y., Snels, M., Viterbini, M., and Quatrevalet, M.: Evaluation of stratospheric ozone, temperature, and aerosol profiles from the LOANA lidar in Antarctica, Polar Science, 6, 209–225, https://doi.org/https://doi.org/10.1016/j.polar.2012.07.001, 2012.

https://doi.org/10.5194/egusphere-2022-972
Preprint. Discussion started: 1 November 2022

Deshler, T., Nardi, B., Adriani, A., Cairo, F., Hansen, G., Fierli, F., Hauchecorne, A., and Pulvirenti, L.: Determining the index of refraction of polar stratospheric clouds above Andoya (69°N) by combining size-resolved concentration and optical scattering measurements, Journal of Geophysical Research: Atmospheres, 105, 3943–3953, https://doi.org/https://doi.org/10.1029/1999JD900469, 2000.

Deshler, T., Hervig, M. E., Hofmann, D. J., Rosen, J. M., and Liley, J. B.: Thirty years of in situ stratospheric aerosol size distribution measurements from Laramie, Wyoming (41°N), using balloon-borne instruments, Journal of Geophysical Research, 108, 4167, 2003a.

Deshler, T., Larsen, N., Weissner, C., Schreiner, J., Mauersberger, K., Cairo, F., Adriani, A., Di Donfrancesco, G., Ovarlez, J., Ovarlez, H., Blum, U., Fricke, K. H., and Dörnbrack, A.: Large nitric acid particles at the top of an Arctic stratospheric cloud, Journal of Geophysical Research: Atmospheres, 108, https://doi.org/https://doi.org/10.1029/2003JD003479, 2003b.

Deshler, T., Luo, B., Kovilakam, M., Peter, T., and Kalnajs, L. E.: Retrieval of Aerosol Size Distributions From In Situ Particle Counter Measurements: Instrument Counting Efficiency and Comparisons With Satellite Measurements, Journal of Geophysical Research: Atmospheres, 124, 5058–5087, https://doi.org/https://doi.org/10.1029/2018JD029558, 2019.

Di Donfrancesco, G., Adriani, A., Gobbi, G., and Cairo, F.: Lidar observations of the stratospheric aerosol during 1993 above McMurdo Station, Antarctica, Journal of Atmospheric and Solar-Terrestrial Physics, 62, 713–723, https://doi.org/https://doi.org/10.1016/S1364-6826(00)00061-4, 2000.

Dubovik, O., Sinyuk, A., Lapyonok, T., Holben, B. N., Mishchenko, M., Yang, P., Eck, T. F., Volten, H., Muñoz, O., Veihelmann, B., van der Zande, W. J., Leon, J.-F., Sorokin, M., and Slutsker, I.: Application of spheroid models to account for aerosol particle nonsphericity in remote sensing of desert dust, J. Geophys. Res., 111, D11 208, https://doi.org/10.1029/2005JD006619, 2006.

Dubovik, O., Lapyonok, T., Litvinov, P., Herman, M., Fuertes, D., Ducos, F., Torres, B., Derimian, Y., Huang, X., Lopatin, A., Chaikovsky, A., Aspetsberger, M., and Federspiel, C.: GRASP: a versatile algorithm for characterizing the atmosphere, SPIE Newsroom, https://doi.org/10.1117/2.1201408.005558, 2014.

Engel, I., Luo, B. P., Pitts, M. C., Poole, L. R., Hoyle, C. R., Grooß, J.-U., Dörnbrack, A., and Peter, T.: Heterogeneous formation of polar stratospheric clouds – Part 2: Nucleation of ice on synoptic scales, Atmospheric Chemistry and Physics, 13, 10 769–10 785, https://doi.org/10.5194/acp-13-10769-2013, 2013.

Freudenthaler, V., Homburg, F., and Jäger, H.: Optical parameters of contrails from lidar measurements: Linear depolarization, Geophysical research letters, 23, 3715–3718, 1996.

Gobbi, G. P.: Lidar estimation of stratospheric aerosol properties: Surface, volume, and extinction to backscatter ratio, Journal of Geophysical Research: Atmospheres, 100, 11 219–11 235, https://doi.org/https://doi.org/10.1029/94JD03106, 1995.

Grooß, J.-U., Engel, I., Borrmann, S., Frey, W., Günther, G., Hoyle, C. R., Kivi, R., Luo, B. P., Molleker, S., Peter, T., Pitts, M. C., Schlager, H., Stiller, G., Vömel, H., Walker, K. A., and Müller, R.: Nitric acid trihydrate nucleation and denitrification in the Arctic stratosphere, Atmospheric Chemistry and Physics, 14, 1055–1073, https://doi.org/10.5194/acp-14-1055-2014, 2014.

Grothe, H., Tizek, H., Waller, D., and Stokes, D. J.: The crystallization kinetics and morphology of nitric acid trihydrate, Physical chemistry chemical physics, 8, 2232–2239, 2006.

Heymsfield, A. J., Kr?mer, M., Luebke, A., Brown, P., Cziczo, D. J., Franklin, C., Lawson, P., Lohmann, U., McFarquhar, G., Ulanowski, Z., and Tricht, K. V.: Cirrus Clouds, Meteorological Monographs, 58, 2.1 – 2.26, https://doi.org/10.1175/AMSMONOGRAPHS-D-16-0010.1, 2017.

Hofmann, D. J. and Deshler, T.: Stratospheric cloud observations during formation of the Antarctic ozone hole in 1989, Journal of Geophysical Research: Atmospheres, 96, 2897–2912, https://doi.org/https://doi.org/10.1029/90JD02494, 1991.

https://doi.org/10.5194/egusphere-2022-972
Preprint. Discussion started: 1 November 2022

Hoyle, C. R., Engel, I., Luo, B. P., Pitts, M. C., Poole, L. R., Grooß, J.-U., and Peter, T.: Heterogeneous formation of polar stratospheric clouds – Part 1: Nucleation of nitric acid trihydrate (NAT), Atmospheric Chemistry and Physics, 13, 9577–9595, https://doi.org/10.5194/acp-13-9577-2013, 2013.

Jumelet, J., Bekki, S., David, C., and Keckhut, P.: Statistical estimation of stratospheric particle size distribution by combining optical modelling and lidar scattering measurements, Atmospheric Chemistry and Physics, 8, 5435–5448, 2008.

Kokhanovsky, A.: Optical properties of terrestrial clouds, Earth-Science Reviews, 64, 189–241, https://doi.org/10.1016/S0012-8252(03)00042-4, 2004.

Larsen, N., Knudsen, B. M., Svendsen, S. H., Deshler, T., Rosen, J. M., Kivi, R., Weisser, C., Schreiner, J., Mauerberger, K., Cairo, F., Ovarlez, J., Oelhaf, H., and Spang, R.: Formation of solid particles in synoptic-scale Arctic PSCs in early winter 2002/2003, Atmospheric Chemistry and Physics, 4, 2001–2013, https://doi.org/10.5194/acp-4-2001-2004, 2004.

Liu, L. and Mishchenko, M. I.: Constraints on PSC particle microphysics derived from lidar observations, Journal of Quantitative Spectroscopy and Radiative Transfer, 70, 817–831, 2001.

Mishchenko, M. I.: Electromagnetic scattering by nonspherical particles: A tutorial review, Journal of Quantitative Spectroscopy and Radiative Transfer, 110, 808–832, https://doi.org/https://doi.org/10.1016/j.jqsrt.2008.12.005, light Scattering: Mie and More Commemorating 100 years of Mie's 1908 publication, 2009.

Mishchenko, M. I. and Travis, L. D.: Capabilities and limitations of a current FORTRAN implementation of the T-matrix method for randomly oriented, rotationally symmetric scatterers, Journal of Quantitative Spectroscopy and Radiative Transfer, 60, 309–324, https://doi.org/https://doi.org/10.1016/S0022-4073(98)00008-9, 1998.

Mishchenko, M. I., Travis, L. D., and Mackowski, D. W.: T-matrix computations of light scattering by nonspherical particles: A review, Journal of Quantitative Spectroscopy and Radiative Transfer, 55, 535–575, 1996.

Peter, T. and Grooß, J.-U.: Chapter 4 Polar Stratospheric Clouds and Sulfate Aerosol Particles: Microphysics, Denitrification and Heterogeneous Chemistry, in: Stratospheric Ozone Depletion and Climate Change, pp. 108–144, The Royal Society of Chemistry, https://doi.org/10.1039/9781849733182-00108, 2012.

Pitts, M. C., Poole, L. R., and Thomason, L. W.: CALIPSO polar stratospheric cloud observations: second-generation detection algorithm and composition discrimination, Atmospheric Chemistry and Physics, 9, 7577–7589, https://doi.org/10.5194/acp-9-7577-2009, 2009.

Pitts, M. C., Poole, L. R., Lambert, A., and Thomason, L. W.: An assessment of CALIOP polar stratospheric cloud composition classification, Atmospheric Chemistry and Physics, 13, 2975–2988, https://doi.org/10.5194/acp-13-2975-2013, 2013.

Pitts, M. C., Poole, L. R., and Gonzalez, R.: Polar stratospheric cloud climatology based on CALIPSO spaceborne lidar measurements from 2006 to 2017, Atmospheric Chemistry and Physics, 18, 10 881–10 913, https://doi.org/10.5194/acp-18-10881-2018, 2018a.

Pitts, M. C., Poole, L. R., and Gonzalez, R.: Polar stratospheric cloud climatology based on CALIPSO spaceborne lidar measurements from 2006 to 2017, Atmospheric Chemistry and Physics, 18, 10 881–10 913, https://doi.org/10.5194/acp-18-10881-2018, 2018b.

Reichardt, J., Reichardt, S., Yang, P., and McGee, T. J.: Retrieval of polar stratospheric cloud microphysical properties from lidar measurements: Dependence on particle shape assumptions, Journal of Geophysical Research: Atmospheres, 107, SOL–25, 2002.

Reichardt, J., Dörnbrack, A., Reichardt, S., Yang, P., and McGee, T. J.: Mountain wave PSC dynamics and microphysics from ground-based lidar measurements and meteorological modeling, Atmospheric Chemistry and Physics, 4, 1149–1165, https://doi.org/10.5194/acp-4-1149-2004, 2004.

Sassen, K. and Hsueh, C.-y.: Contrail properties derived from high-resolution polarization lidar studies during SUCCESS, Geophysical research letters, 25, 1165–1168, 1998.

https://doi.org/10.5194/egusphere-2022-972
Preprint. Discussion started: 1 November 2022

Scarchilli, C., Adriani, A., Cairo, F., Donfrancesco, G. D., Buontempo, C., Snels, M., Moriconi, M. L., Deshler, T., Larsen, N., Luo, B., Mauersberger, K., Ovarlez, J., Rosen, J., and Schreiner, J.: Determination of polar stratospheric cloud particle refractive indices by use of in situ optical measurements and T-matrix calculations, Appl. Opt., 44, 3302–3311, https://doi.org/10.1364/AO.44.003302, 2005.

Singham, S. B. and Salzman, G. C.: Evaluation of the scattering matrix of an arbitrary particle using the coupled dipole approximation, The Journal of Chemical Physics, 84, 2658–2667, https://doi.org/10.1063/1.450338, 1986.

Snels, M., Cairo, F., Colao, F., and Di Donfrancesco, G.: Calibration method for depolarization lidar measurements, International Journal of Remote Sensing, 30, 5725–5736, 2009.

Snels, M., Cairo, F., Di Liberto, L., Scoccione, A., Bracaglia, M., and Deshler, T.: Comparison of Coincident Optical Particle Counter and Lidar Measurements of Polar Stratospheric Clouds Above McMurdo (77.85° S, 166.67° E) From 1994 to 1999, Journal of Geophysical Research: Atmospheres, 126, e2020JD033 572, 2021.

Solomon, S.: The mystery of the Antarctic ozone "hole", Reviews of Geophysics, 26, 131–148, 1988.

Toon, O. B., Tabazadeh, A., Browell, E. V., and Jordan, J.: Analysis of lidar observations of Arctic polar stratospheric clouds during January 1989, Journal of Geophysical Research: Atmospheres, 105, 20 589–20 615, 2000.

Tritscher, I., Grooß, J.-U., Spang, R., Pitts, M. C., Poole, L. R., Müller, R., and Riese, M.: Lagrangian simulation of ice particles and resulting dehydration in the polar winter stratosphere, Atmospheric Chemistry and Physics, 19, 543–563, https://doi.org/10.5194/acp-19-543-2019, 2019.

Tritscher, I., Pitts, M. C., Poole, L. R., Alexander, S. P., Cairo, F., Chipperfield, M. P., Grooß, J.-U., Höpfner, M., Lambert, A., Luo, B., Molleker, S., Orr, A., Salawitch, R., Snels, M., Spang, R., Woiwode, W., and Peter, T.: Polar Stratospheric Clouds: Satellite Observations, Processes, and Role in Ozone Depletion, Reviews of Geophysics, 59, e2020RG000 702, https://doi.org/https://doi.org/10.1029/2020RG000702, e2020RG000702 2020RG000702, 2021.

Um, J. and McFarquhar, G. M.: Dependence of the single-scattering properties of small ice crystals on idealized shape models, Atmospheric Chemistry and Physics, 11, 3159–3171, https://doi.org/10.5194/acp-11-3159-2011, 2011.

Voigt, C., Schreiner, J., Kohlmann, A., Zink, P., Mauersberger, K., Larsen, N., Deshler, T., Kröger, C., Rosen, J., Adriani, A., et al.: Nitric acid trihydrate (NAT) in polar stratospheric clouds, Science, 290, 1756–1758, 2000.

Voigt, C., Larsen, N., Deshler, T., Kröger, C., Schreiner, J., Mauersberger, K., Luo, B., Adriani, A., Cairo, F., Di Donfrancesco, G., Ovarlez, J., Ovarlez, H., Dörnbrack, A., Knudsen, B., and Rosen, J.: In situ mountain-wave polar stratospheric cloud measurements: Implications for nitric acid trihydrate formation, Journal of Geophysical Research: Atmospheres, 108, https://doi.org/https://doi.org/10.1029/2001JD001185, 2003.

Weisser, C., Mauersberger, K., Schreiner, J., Larsen, N., Cairo, F., Adriani, A., Ovarlez, J., and Deshler, T.: Composition analysis of liquid particles in the Arctic stratosphere under synoptic conditions, Atmospheric Chemistry and Physics, 6, 689–696, https://doi.org/10.5194/acp-6-689-2006, 2006.

Woiwode, W., Höpfner, M., Bi, L., Pitts, M. C., Poole, L. R., Oelhaf, H., Molleker, S., Borrmann, S., Klingebiel, M., Belyaev, G., Ebersoldt, A., Griessbach, S., Grooß, J.-U., Gulde, T., Krämer, M., Maucher, G., Piesch, C., Rolf, C., Sartorius, C., Spang, R., and Orphal, J.: Spectroscopic evidence of large aspherical β-NAT particles involved in denitrification in the December 2011 Arctic stratosphere, Atmospheric Chemistry and Physics, 16, 9505–9532, https://doi.org/10.5194/acp-16-9505-2016, 2016.

Yang, P. and Liou, K. N.: Finite-difference time domain method for light scattering by small ice crystals in three-dimensional space, J. Opt. Soc. Am. A, 13, 2072–2085, https://doi.org/10.1364/JOSAA.13.002072, 1996a.

https://doi.org/10.5194/egusphere-2022-972
Preprint. Discussion started: 1 November 2022

Yang, P. and Liou, K. N.: Geometric-optics–integral-equation method for light scattering by nonspherical ice crystals, Appl. Opt., 35, 6568–6584, https://doi.org/10.1364/AO.35.006568, 1996b.

Yang, P. and Liou, K.-N.: Light scattering and absorption by nonspherical ice crystals, pp. 31–71, Springer Berlin Heidelberg, Berlin, Heidelberg, https://doi.org/10.1007/3-540-37672-0_2, 2006.

Young, A. T.: Revised depolarization corrections for atmospheric extinction, Appl. Opt., 19, 3427–3428, https://doi.org/10.1364/AO.19.003427, 1980.

https://doi.org/10.5194/egusphere-2022-972
Preprint. Discussion started: 1 November 2022

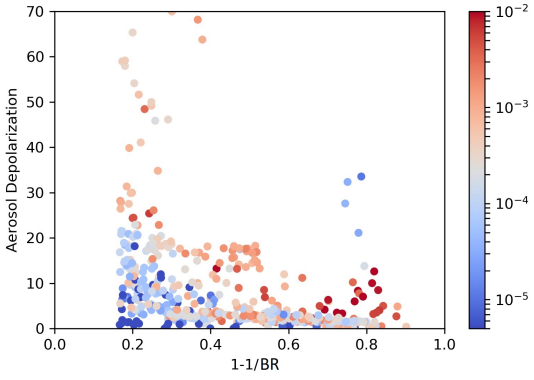

Figure 1. Scatterplot of aerosol depolarization vs 1-1/BR, where BR is the Backscatter Ratio. Data are from McMurdo lidar and Kiruna balloon flights backscattersonde, coincident with balloonborne OPC PSD measurements, fitted with mono or bimodal lognormals. The color codes the fraction of particles with radius larger than 1 μm with respect to the total number of particles in the PSDs. We reports data points with BR greater than 1.2, β_A^{cross} greater than 5 $10^{-6} km^{-1} sr^{-1}$ and temperature at the observation below 200 K.

https://doi.org/10.5194/egusphere-2022-972
Preprint. Discussion started: 1 November 2022

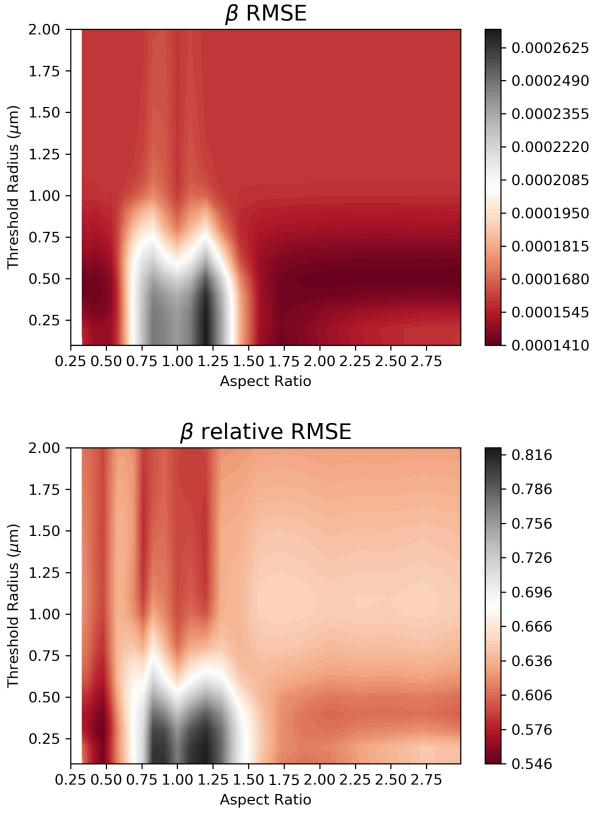

Figure 2. Contour plot of the RMSE (upper panel) and relative RMSE (lower panel) of the measured and modelled aerosol backscatter coefficient β_A.

https://doi.org/10.5194/egusphere-2022-972
Preprint. Discussion started: 1 November 2022

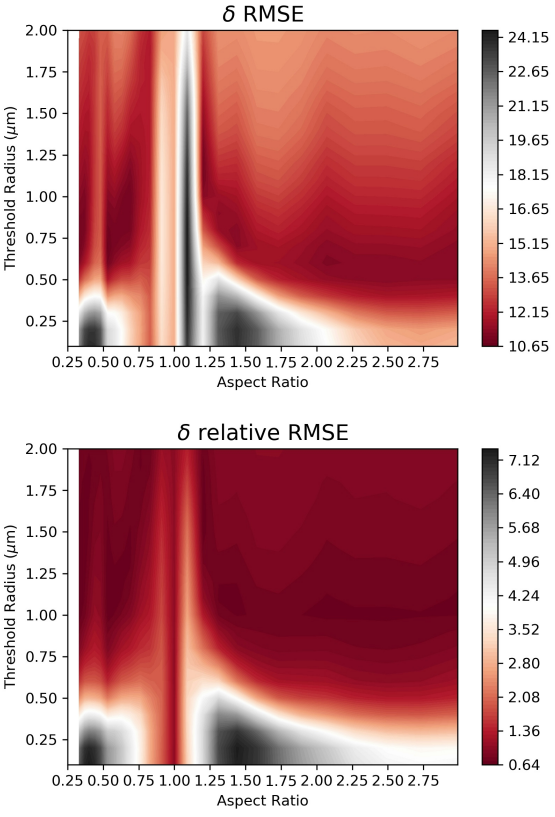

Figure 3. Contour plot of the RMSE (upper panel) and relative RMSE (lower panel) of the measured and modelled aerosol depolarization δ_A.

https://doi.org/10.5194/egusphere-2022-972
Preprint. Discussion started: 1 November 2022

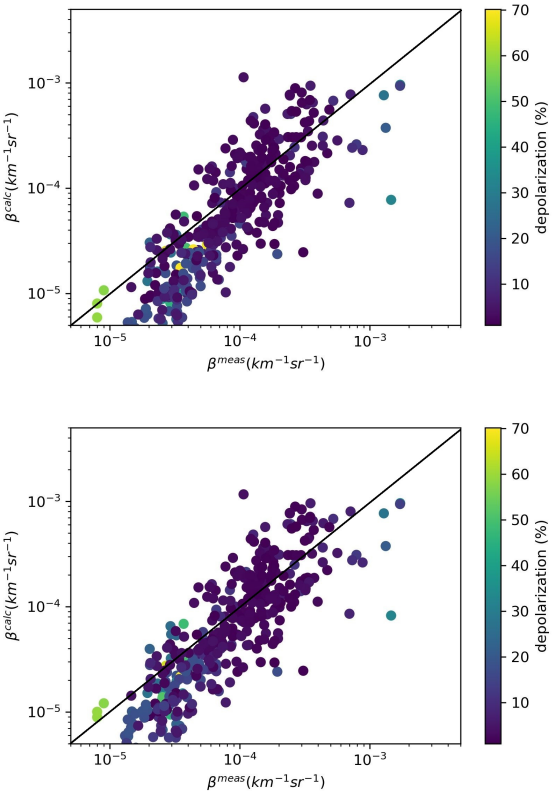

Figure 4. Scatterplot of computed vs measured particle backscatter coefficients β_A. In the upper panel, AR=2 and R_{th} =1.0 μm were used; in the lower panel AR was changed to 0.5. We reports data points with BR greater than 1.2, β_A^{cross} greater than 5 $10^{-6}km^{-1}sr^{-1}$ and temperature at the observation below 200 K. The colour codes the corresponding δ_A value.

https://doi.org/10.5194/egusphere-2022-972
Preprint. Discussion started: 1 November 2022

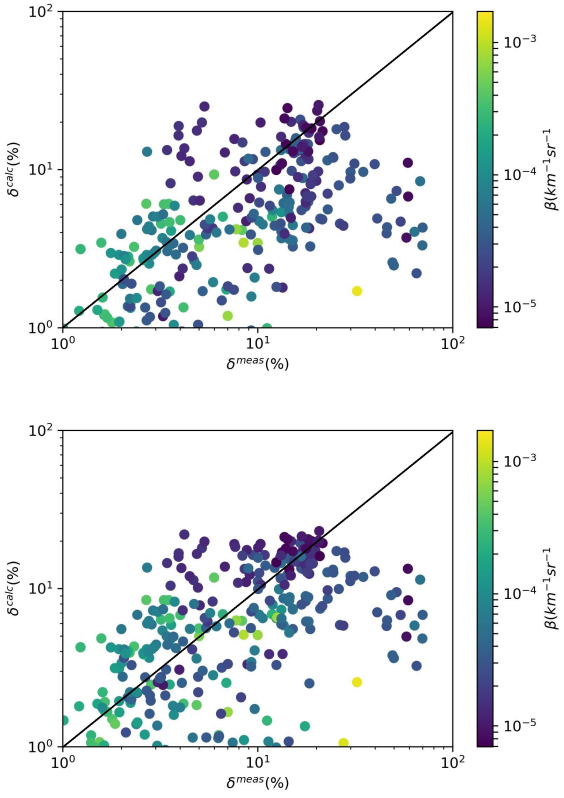

Figure 5. Scatterplot of computed vs measured particle backscatter coefficients δ_A. In the upper panel, AR=2 and R_{th} =1.0 μm were used; in the lower panel AR was changed to 0.5. We reports data points with BR greater than 1.2, β_A^{cross} greater than 5 $10^{-6}km^{-1}sr^{-1}$ and temperature at the observation below 200 K. The colour codes the corresponding β_A value.

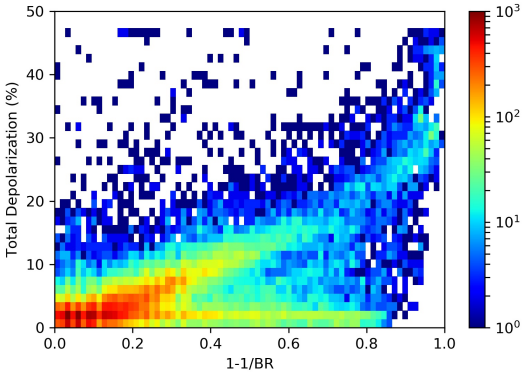

Figure 6. 2D historam of Total Volume Depolarization δ_{TA} vs 1-1/BR, where BR is the Backscatter Ratio. Data are from McMurdo lidar and cover the winters from 1990 to 2002. The color codes the number of observations.